Long-memory Log-linear Zero-inflated Generalized Poisson Autoregression for Covid-19 Pandemic Modeling

Xiaofei Xu[1], Yijiong Zhang[2], Yan Liu[3], Yuichi Goto[4], Masanobu Taniguchi[5], and Ying Chen[2]

[1] *School of Mathematics and Statistics, Wuhan University, People's Republic of China*

[2]*Department of Mathematics, National University of Singapore, Singapore*

[3]*Institute for Mathematical Science, Waseda University, Japan*

[3]*Faculty of Science and Engineering,Waseda University, Japan*

[4]*Faculty of Mathematics, Kyushu University, Japan*

[5] *Research Institute for Science and Engineering, Waseda University, Japan*

Abstract:

This paper describes the dynamics of daily new cases arising from the Covid-19 pandemic using a long-range dependent model. A new long memory model, LFIGX (Log-linear zero-inflated generalized Poisson integer-valued Fractionally Integrated GARCH process with eXogenous covariates), is proposed to account for count time series data with a long-run dependent effect. It provides a novel unified framework for integer-valued processes with serial and long-range dependence (positive or negative), over-dispersion, zero-inflation, nonlinearity, and exogenous variable effects. We adopt an adaptive Bayesian Markov Chain Monte Carlo (MCMC) sampling scheme for parameter estimation. This new modeling is applied to the daily new confirmed cases of the Covid-19 pandemic in six countries including Japan, Vietnam, Italy, the United Kingdom, Brazil, and the United States. The LFIGX model provides insightful interpretations of the impacts of policy index and temperature and delivers good forecasting performance for the dynamics of the daily new cases in different countries.

1. Introduction

The Covid-19 pandemic has disastrously caused an enormous global human health problem and economy disruption since December 2019. The World Health Organization has reported more than 350 million Covid-19 confirmed cases in over 200 countries, including about 5.1 million deaths as of mid-January 2022. There has been abundant literature studying the Covid-19 pandemic across multiple disciplines since the outbreak; See, e.g., the macroeconomic and societal impact of Covid-19 (Ludvigson et al., 2020; Atkeson, 2020; Chakraborty and Maity, 2020), concerns and effects of the Covid variants (Vaidyanathan, 2021; Volz et al., 2021; Faria et al., 2021), dynamic modeling of new cases, deaths, or infection rate of Covid-19 (Lin et al., 2020; Jiang et al., 2020; Agosto et al., 2021; Roy and Karmakar, 2021; Li and Linton, 2021), and the effect of exogenous factors on the Covid-19 pandemic (Dandekar and Barbastathis, 2020; Chen et al., 2021; Chernozhukov et al., 2021). In particular, the effect of containment policies on the transmission of the Covid-19 virus has been widely studied, with mixed findings under various cultural and health conditions or in different frameworks of modeling and covariates, see e.g. Hsiang et al. (2020), Chernozhukov et al. (2021), and Chen et al. (2021). Han et al. (2022) and Qiu et al. (2020) argued that a country's new case growth of Covid-19 increases with higher temperatures due to the encouragement of social activity and gatherings under warm weather. While Shi et al. (2020) and Mecenas et al. (2020) have presented that cold weather leads to

higher level of incidences as such weather conditions potentiate the spread of the Covid-19 virus. While these studies are insightful with mixed findings, they do not investigate the long-range dependence of Covid-19 pandemic, or analyze the effects of multiple factors simultaneously in a long-range dependent framework. In this paper, we investigate the long-range dependence and the effects of multiple exogenous covariates on daily new Covid-19 cases. We examine the temperature and policy effectiveness in terms of both immediate impact, namely, in the following one and two days, and intermediate impact after one and two weeks since the policy's initiation in a unified long memory framework. Furthermore, it is important to capture the developing trend of newly confirmed Covid-19 cases, not only for short terms e.g. one- or two-day-ahead but also for the intermediate terms e.g. 7- and 14-day ahead. These features are useful for people's activities and government policy determination. Therefore, we conduct multiple steps ahead forecasting for six countries across four continents.

The counts of daily new Covid-19 cases are discrete and integer-valued, exhibiting features of over-dispersion and serial correlation and could also be influenced by exogenous factors such as lockdown and wearing mask polices simultaneously. Statistical analysis of count time series has been an active research area, covering a broad range of studies and implementations from the incidence of epidemiology and pandemics to criminal incidents, queueing systems and insurance claims (Davis and Dunsmuir, 2016; Chen and Lee, 2016). Among others, Ferland et al. (2006) proposed the integer-valued generalized autoregressive conditional heteroscedastic model with Poisson deviates (P-INGARCH), which is commonly used model for the count time series with overdispersion. The P-INGARCH models are further

generalized with, e.g., the log-linear P-INGARCH (Fokianos and Tjøstheim, 2011, 2012) and generalized Poisson/negative binomial/zero-inflated Poisson-INGARCH(X) models (Famoye and Singh, 2006; Zhu, 2011; Chen and Lee, 2016; Xu et al., 2020). A comprehensive methodological review of count time series modeling refers to Davis et al. (2021) and the references therein. However, these works focus on modeling count time series in a short-memory framework, which is unable to achieve or produce long-memory process. The slow decay phenomenon in the sample autocorrelation is exhibited in the Covid-19 pandemic data, which may be ascribed to the long-range dependence or a long-memory property.

The study of long-memory phenomenon dates back to Hurst (1951) in explaining the long-range dependence in the record of the Nile River. Granger (1980) suggested that aggregation of short-memory processes could lead to a long-memory time series. Fractionally integrated processes have frequently been considered for their hyperbolically decaying shock propagation in the literature of long memory. A typical example is the fractional integrated generalized autoregressive conditional heteroscedaticity (FIGARCH) model proposed by Baillie et al. (1996), which displays better empirical performance in modeling stock return volatility processes opposed to a standard GARCH model. The autoregressive fractional integrated moving average (ARFIMA) process (Granger and Joyeux, 1980; Bhardwaj and Swanson, 2006) has also emerged as a prevalent model for long-range dependent time series, especially in volatility process modeling. However, there is limited study on long memory modeling for integer-valued time series. Quoreshi (2014) proposed an integer-valued ARFIMA model to capture the long-memory aspects of high-frequency stock transaction numbers. Livsey et al. (2018) extended the vector ARFIMA model to

bivariate integer-valued case with an application to the annual number of major hurricanes, see also Darolles et al. (2019) and Quoreshi (2017). As for the extension of FIGARCH to count time series, Segnon and Stapper (2019) considered an integer-valued FIGARCH process with the Poisson distribution (P-INFIGARCH). However, this model cannot capture the multiple features of count time series, e.g., over/under-dispersion, nonlinearity and the effects of exogenous covariates.

In this paper, we focus on a new synthetic methodology for modeling the long-range dependence phenomenon with periodic behavior for the Covid-19 daily new cases series. We propose a log-linear zero-inflated generalized Poisson integer-valued fractionally integrated GARCH model with exogenous covariates (LFIGX) to capture multiple features of daily Covid-19 new cases in a long memory framework. Existing INGARCH with Poisson or generalized Poisson type models can only handle short memory features. Note that Segnon and Stapper (2019) also considered the P-INFIGARCH model but without exogenous variables, and it cannot handle over-dispersion, zero-inflation, and nonlinearity. The question on the true source of long memory diagnosis still remains a question (Chen et al., 2010), and the presence of structural breaks can lead to misleading inference regarding long memory diagnosis (Diebold, 1986; Lamoureux and Lastrapes, 1990; Mikosch and Stărică, 2004). Instead of using short memory with breaks or time-varying models (Xu et al., 2020; Chen and Lee, 2016), we consider long memory modeling for Covid-19 data, not only because it is natural to introduce long-range dependence for the intensity for Covid-19 count series due to the aggregation of possible numerous latent Covid-19 infectors (Granger, 1980), but also because it has practical implications for future policy design and long-term prediction.

The proposed LFIGX model incorporates a long-memory integer-valued FIGARCH model with exogenous covariates for the intensity of Covid-19 count time series, and zero-inflated generalized Poisson distribution is applied to allow for possible over-dispersion and zero-inflation features. Hence, the model is flexible to describe the dynamics of daily new Covid-19 case series with mixed features of serial dependence (positive or negative), over-dispersion, zero-inflation, nonlinearity, exogenous covariates impact, and long-memory in a unified framework. Bayesian method is adopted for parameter estimation based on adaptive MCMC procedure. The Bayesian inference for LFIGX model is advantageous because it provides a way of estimation and prediction taking into account parameter uncertainty and prior knowledge of a stochastic process. Bollerslev and Mikkelsen (1996) and Baillie et al. (1996) have proved asymptotic consistency and normality properties of the quasi maximum likelihood estimators (qMLE) under sufficient nonnegativity conditions of conditional variance for the FIGARCH process in the modeling of high-frequent volatility process, and Conrad and Haag (2006) extended these results of nonnegativity parameter conditions to higher-order cases, which were adopted by Segnon and Stapper (2019) for estimation of the P-INFIGARCH model. Though our paper adopts Bayesian method and involves a different distribution, the numerical study demonstrates reasonably good estimation performance for the LFIGX model. We apply the LFIGX model to the Covid-19 daily new cases data from six countries across four continents and conduct a comprehensive analysis to their dynamics and the effects of exogenous covariates. Our analysis provides insightful interpretations on the short and intermediate term impacts of policy index and temperature, and delivers good multiple step ahead forecasting performance for the dynamics of

Covid-19 daily new cases.

Our contributions include the following. 1) We propose a new synthetic LFIGX model for the long-range dependent count time series, which enables us to account for a number of features in a unified framework and simultaneously incorporate the impact of multivariate exogenous covariates. In comparison, existing works only consider a subset of the features and/or do so under a short memory framework. 2) We demonstrate the application of Bayesian MCMC sampling method for parameter estimation of FIGARCH type models for count time series. The existing literature of integer-valued long memory modeling, e.g. INARFIMA model (Quoreshi, 2014) and P-INFIGARCH (Segnon and Stapper, 2019) all utilize the qMLE methods. 3) We provide an interpretable estimation of the stochastic intensity of the Covid-19 daily new cases and the short/middle-term impacts of multivariate environmental and policy variables.

The rest of this paper is organized as follows. Section 2 describes the daily new Covid-19 cases data and the exogenous variables. Section 3 presents the LFIGX model and the parameter estimation procedure using the Bayesian MCMC sampling technique. Section 4 investigates the finite sample performance of the LFIGX model under various scenarios. In Section 5, we demonstrate the real data analysis to the daily news cases of Covid-19 pandemic in six countries. Section 6 concludes.

2. The Covid-19 Data

We consider daily new cases of Covid-19 in six countries with a wide spectrum across four continents, respectively. Asian countries suffered the first outbreak of the Covid-

19 pandemic since December 2019, we consider two Asian countries: Japan (JPN) and Vietnam (VNM) as illustrations. We also choose two American countries, the United States (USA) which has the largest amount of accumulated confirmed cases and deaths, and Brazil (BRA) which ranks third in terms of total number of confirmed cases and deaths globally (till 4 January 2022). Lastly, we select two countries from Europe: Italy (ITA), which suffers from the first outbreak in Europe, and the United Kingdom (GBR) which has the most accumulated cases among the European countries (till 4 January 2022).

The primary data sources include daily new Covid-19 cases, policy indicators, and temperature. We collected the daily new cases data of six representative countries from Our World in Data website maintained by the University of Oxford. We also obtain the containment and health index as policy indicator variable from there. The index on any given day takes a value between 0 and 100 with a higher score indicating a stricter government policy. We collect the daily mean temperature from the National Oceanic and Atmospheric Administration (NOAA). The NOAA records raw temperature data by several stations from various locations within each country. We take the daily average of the temperatures that are completely recorded from different stations in a country to use except USA. For USA, we select four representative states: California, New Jersey, Texas, and Minnesota, and take the average temperature of the four states to use, considering the large lead are of USA. Meanwhile, to investigate the weekly seasonality of new Covid-19 counts, especially the weekday and weekend effect, we add a dummy variable $D_t = 1$ if the day is Saturday,

---

Our World in Data: `https://ourworldindata.org/coronavirus-source-data`. The index is constructed from taking the weighted sum over a group of policy categories such as school closures, workplace closures, face coverings and testing policy. The detailed categories of policies considered refer to Our World in Data website.

or Sunday, and equals zero otherwise.

Table 1 reports the descriptive statistics of the daily new Covid-19 cases in each country. It is obvious that these six series are all overdispersed with the sample variance much larger than the mean, and ratio ranges from $7.42(\times 10^3)$ to $4.49(\times 10^4)$. The daily new cases at VNM has 19.09% of zeros which indicates the feature of excess zeros, while for other five datasets, there are no or few number of zeros. Meanwhile, the magnitude of counts series is much larger for ITA, GBR, BRA, and USA than the values of two Asian countries.

Table 1: Description and summary statistics of daily new cases.

Dataset(Code)	Period	n	Min	Max	Mean	Variance	Variance/Mean	0s %
Japan(JPN)	2020/1/23∼2022/1/13	722	0	$2.59(\times 10^4)$	$2.50(\times 10^3)$	$1.86(\times 10^7)$	$7.42(\times 10^3)$	1.38
Vietnam(VNM)	2020/1/23∼2022/1/14	723	0	$3.91(\times 10^4)$	$2.75(\times 10^3)$	$2.88(\times 10^7)$	$1.05(\times 10^4)$	19.09
Italy(ITA)	2020/2/21∼2022/1/11	691	17	$2.20(\times 10^5)$	$1.13(\times 10^4)$	$5.05(\times 10^8)$	$4.49(\times 10^4)$	0
United Kingdom(GBR)	2020/1/31∼2022/1/4	705	0	$2.21(\times 10^5)$	$1.94(\times 10^4)$	$6.93(\times 10^8)$	$3.57(\times 10^4)$	1.41
United States(USA)	2020/1/23∼2022/1/9	718	0	$1.07(\times 10^6)$	$8.40(\times 10^4)$	$1.02(\times 10^{10})$	$1.21(\times 10^4)$	3.76
Brazil (BRA)	2020/2/26∼2021/12/10	654	0	$1.24(\times 10^5)$	$3.38(\times 10^4)$	$5.97(\times 10^8)$	$1.76(\times 10^4)$	1.2

Figures 1 and 2 display the time series plot and autocorrelation functions (ACF) plot of the daily new cases of Covid-19, respectively. We can find different dynamic patterns in, e.g., trend, intensity, duration, and frequency of waves, as well as ACF decays of these countries. For example, both JPN and USA suffer six waves from January 2020 to January 2022, while USA develops more volatile intensity than JPN at last two waves. VNM shows only two waves and remains stable at low level until June 2021 when a sharp increment occurs. The data of BRA fluctuates seriously with largest volatility among 6 countries during the whole period. In Figure 2, the ACF plots show the slower decay for VNM and GBR, which may reveal a long-dependent feature of the data. JPN and ITA decrease to be insignificant at around lag 40, while BRA monotonously decreases but still exhibits significant ACF till lag 100. The weekly seasonality is more obvious in BRA and USA. The

values, dynamics, and ACFs of the daily new Covid-19 case series vary from one country to another, which increases the complexity of modeling in a unified framework. The multiple features and complex dynamics in the empirical data require a comprehensive model that can effectively handle the long-range or short-range dependence and over-dispersion simultaneously.
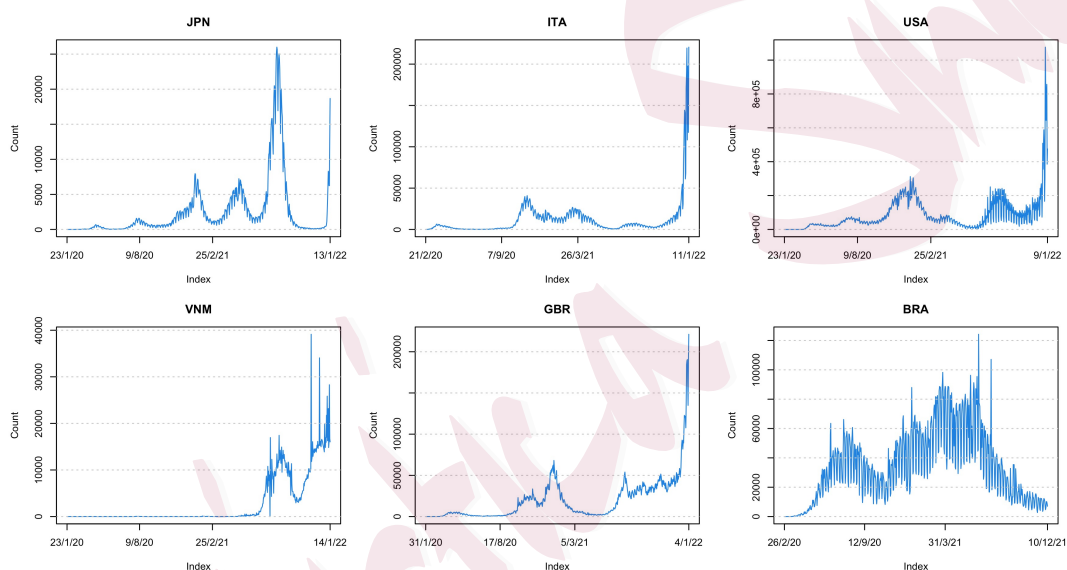

Figure 1: Time series plots of the daily new cases of the Covid-19 pandemic at six countries.

Figure 3 displays the time series plots of the two exogenous variables for JPN, ITA, and USA, as illustration. The graphical demonstration of other countries refers to Figure A in Supplementary Materials. The policy index reveals a sharp increasing trend first and remains relatively stable after that in each country. The strictness of government policy is strongest in ITA and weakest in JPN among these three countries. The temperature series exhibit strong seasonality patterns with higher values at corresponding summer seasons and lower values at winters.
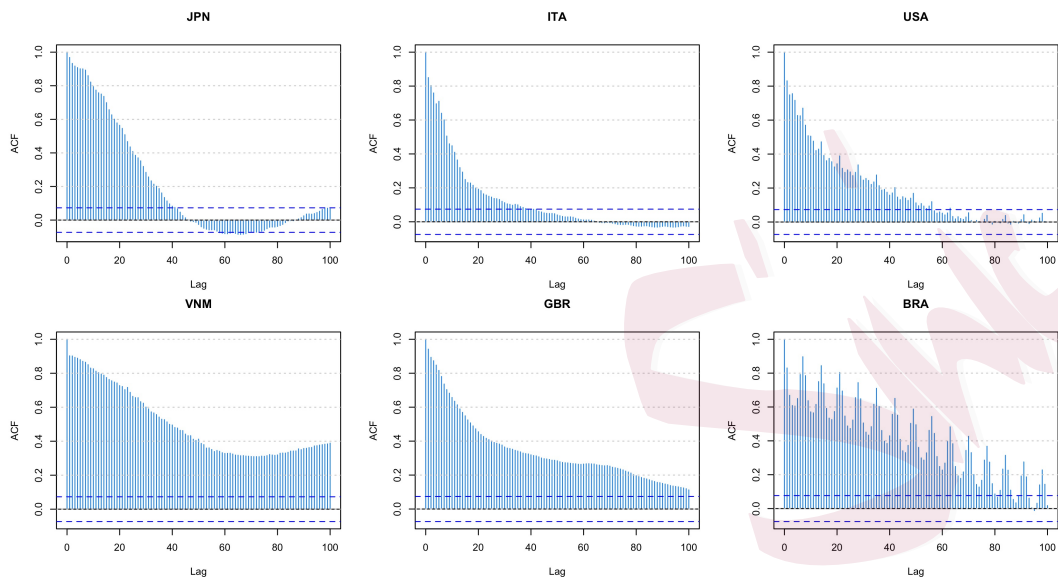
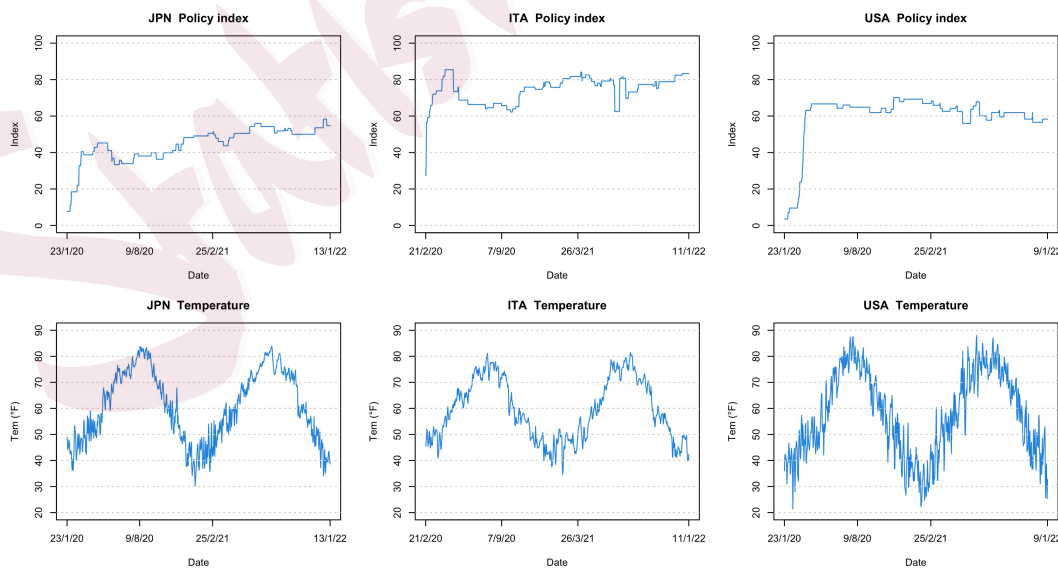Figure 2: The sample ACF plots of the daily new cases of the Covid-19 pandemic at six countries.

Figure 3: The policy index and temperature at JPN, ITA, and USA.

3.   Model and Methodology

In this section, we introduce the **L**og-linear zero-inflated generalized Poisson integer-valued **F**ractionally **I**ntegrated **G**ARCH with e**X**ogenous covariates model with order p, q and fractional parameter d (LFIGX(p, d, q)). The model is flexible to handle the dynamics of the daily Covid-19 new case series with features of autocorrelation, heteroscedasticity, over-dispersion, excess zero observations, and effects of exogenous covariates simultaneously in a long-range dependent framework.

3.1   The **LFIGX**(p, d, q) model

A random variable Y follows a zero-inflated generalized Poisson (ZIGP) distribution (Gupta et al., 1996) with parameters λ, ρ, and φ whose probability density function is given by

$$P(Y = y) = \begin{cases} \rho + (1 - \rho)e^{-\lambda} & \text{if } y = 0 \\[2mm] (1 - \rho)\lambda(\lambda + \varphi y)^{y-1}e^{-(\lambda + \varphi y)}/y! & \text{if } y = 1, 2, \ldots \\[2mm] 0 & \text{for } y > m \text{ if } \varphi < 0, \end{cases}$$

where $\lambda > 0$, $0 \leq \rho < 1$, $\max(-1, -\lambda/m) < \varphi < 1$, and $m(\geq 4)$ is the largest positive integer to satisfy $\lambda + \varphi m > 0$ when $\varphi < 0$. The distribution reduces to the generalized Poisson distribution when $\rho = 0$, and to the Poisson distribution when $\rho = \varphi = 0$. We refer to Xu et al. (2020) for more discussions of the ZIGP distribution.

If a random variable $Y \sim \text{ZIGP}(\lambda, \rho, \varphi)$, the conditional expectation and variance are:

$$\text{E}(Y) = \frac{1-\rho}{1-\varphi}\lambda, \text{ and } \text{Var}(Y) = (1-\rho)\left[\frac{\rho\lambda^2}{(1-\varphi)^2} + \frac{\lambda}{(1-\varphi)^3}\right].$$

It is straightforward to find that variance of Y is greater than the mean (i.e. over-dispersion) if $0 \le \varphi < 1$. When $\rho = 0$, the variance is equal or smaller than the mean when $\varphi = 0$ or $\varphi < 0$ respectively.

Let $\{Y_t; \ t = 1, \ldots, n\}$ denote a count series that is conditionally ZIGP distributed with mean λ_t, such as the daily new cases of Covid-19 pandemic. Let $X_t = (x_{t,1}, \ldots, x_{t,K})^\top$ be the K exogenous covariates. In our study, the exogenous covariates include the policy index, temperature, and a weekend dummy. Let $\mathbf{Y}_t$ and $\mathbf{X}_t$ denote all the past count and exogenous variables' observations at time t, respectively. The family of log-linear INGARCH(p, q) models for intensity λ_t has been widely studied (see e.g. Fokianos and Tjøstheim, 2011), which is defined as:

$$
\begin{aligned}
\log(\lambda_t) &= \omega + \sum_{k=1}^{p} \alpha_k \log(Y_{t-k} + 1) + \sum_{k=1}^{q} \beta_k \log(\lambda_{t-k}) \\
&= \omega + \alpha(L)\log(Y_t + 1) + \beta(L)\log(\lambda_t) \\
\text{rearranging} \quad \log(\lambda_t) &= \frac{\omega}{1-\beta(1)} + \left\{1 - \frac{\Phi^*(L)}{1-\beta(L)}\right\}\log(Y_t + 1),
\end{aligned}
\tag{3.1}
$$

where L denotes the lag or backshift operator, i.e, $L^i x_t \equiv x_{t-i}$. Here $\alpha(L) = \sum_{k=1}^{p} \alpha_k L^k$ and $1 - \beta(L) = 1 - \sum_{k=1}^{q} \beta_k L^k$ are lag polynomials with the roots assumed to lie outside the unit circle, and $\Phi^*(L) = 1 - \beta(L) - \alpha(L)$. The log-intensity $\log(\lambda_t)$ is adopted which relaxes the restriction that both sides should be positive.

In many applied works of the GARCH(p, q) model, the estimated lag polynomial $\Phi^*(x) = 0$ has a root which is statistically indistinguishable from unity (Bollerslev and Mikkelsen, 1996). For example, we found that $\alpha_1 + \beta_1 = 0.981$ using INGARCH(1,1) model for the daily new Covid-19 cases in GBR. While the formulation of model (3.1) has geometric memory, which is only suitable for the short-memory phenomena. Motivated by this empirical regularity, if the polynomial $\Phi^*(L)$ has a unit root and therefore it can be factored as $\Phi^*(L) = \Phi(L)(1 - L)$, where $\Phi(L)$ has all the roots outside the unit circle. Engle and Bollerslev (1986) proposed the so-called Integrated GARCH, or IGARCH process, which exhibits infinite dependence on initial conditions, indicating complete persistence of shocks to the intensity. While it is possible that shocks to the intensity could be highly persistent, i.e., a slow hyperbolic decay, but nevertheless transitory. For example, in Figure 2, the sample ACF of VNM tends to decay more slowly than exponential rate. To cope with such long-range dependence, Baillie et al. (1996) introduced the so-called FIGARCH model, which replaces the first difference operator $(1 - L)$ in $\Phi^*(L)$ with the fractional differencing operator $(1 - L)^d$, where d is a fraction $0 < d < 1$.

Taking into account of these modeling properties and the unique features of count time series, we propose to combine the ZIGP distribution and a nonlinear structure to accommodate zero-inflation, over-dispersion and positive/negative association as well as the effects of exogenous covariates in a long memory framework. The proposed LFIGX(p, d, q)

model is defined as

$$
Y_t | (F_{t-1}^{(y)}, \mathbf{X}_{t-1}) \sim \mathrm{ZIGP}(\lambda_t^*, \varphi, \rho),
$$
$$
\lambda_t^* = \frac{1-\varphi}{1-\rho} \lambda_t, \;\; \log(\lambda_t) = \eta + \left(1 - \frac{\Phi(L)(1-L)^d}{1-\beta(L)}\right) \log(Y_t + 1) + \sum_{k=1}^{K} \gamma_k X_{t-1,k}, \tag{3.2}
$$

where $0 \le \rho < 1$, $\max(-1, -\lambda_t^*/m) < \varphi < 1$, $m (\ge 4)$ is again the largest positive integer

for which $\lambda_t^* + \varphi m > 0$ when $\varphi < 0$. Here, $F_{t-1}^{(y)}$ is the σ-fields generated by previous

observations $\{Y_{t-1}, \ldots, Y_1\}$. We consider $0 \le \varphi < 1$ for the over-dispersion case. Note

that Segnon and Stapper (2019) also considered an INFIGARCH model for count time

series, yet cannot handle possible over-dispersion, zero-inflation and nonlinear dependence

features by using Poisson distribution and without exogenous variables as well.

Denote the lag polynomial $\psi(L)$ as

$$
\psi(L) = 1 - \frac{\Phi(L)(1-L)^d}{1-\beta(L)} = \sum_{k=1}^{\infty} \psi_k L^k \; (say),
$$

we set $0 < d \le 0.5$ accounting for the finite variance of $\log(Y_t + 1)$ series (Taniguchi and

Kakizawa, 2000) and all the roots of $\Phi(L)$ and $1 - \beta(L)$ lie outside the unit circle. The

fractional differencing operator $(1-L)^d$ can be written in terms of hypergeometric function:

$$
(1-L)^d = F(-d, 1, 1; L) = \sum_{k=0}^{\infty} \frac{\Gamma(k-d)}{\Gamma(k+1)\Gamma(-d)} L^k := \sum_{k=0}^{\infty} \delta_{d,k} L^k,
$$

where $\delta_{d,0} = 1$. It is noted that the dependence is driven by the coefficients in $\psi(L)$ in model

(3.2), which allows for the investigation of the temporal dependence of intensity and the

memory of the process on the past observations. The lag coefficients $\psi(L)$ in the infinite

ARCH representation are approximately $\psi_k \sim ck^{-d-1}$, where c is a positive constant (Kılıç,

2011). Hence the log-intensity can be expressed as the distributed lag of past observations

with coefficients decaying at a hyperbolic rate, which makes it distinctively different from

the short (geometric) memory models like the GARCH and IGARCH models.

We intensively discuss the derivation and estimation of LFIGX$(1,d,1)$ model, since the

FIGARCH$(1,d,1)$ model is definitely the most often used specification and appears to be

particularly useful in empirical applications. To be specific, the LFIGX$(1,d,1)$ model is

defined as

$$
\begin{aligned}
Y_t|(F_{t-1}^{(y)}, \mathbf{X}_{t-1}) &\sim \text{ZIGP}(\lambda_t^*, \varphi, \rho), \\
\lambda_t^* = \frac{1-\varphi}{1-\rho}\lambda_t, \quad \log(\lambda_t) &= \eta + \left(1 - \frac{(1-\phi_1 L)(1-L)^d}{1-\beta_1 L}\right)\log(Y_t + 1) + \sum_{k=1}^{K}\gamma_k X_{t-1,k}.
\end{aligned}
\tag{3.3}
$$

Equating autoregression coefficients of the lag operator $\psi(L)$ in model (3.3), we have

$$
\begin{aligned}
\psi_1 &= \phi_1 - \beta_1 + d, \\
\psi_k &= \beta_1\psi_{k-1} + \left(\frac{k-1-d}{k} - \phi_1\right)\delta_{d,k-1}, \text{ for all } k \geq 2.
\end{aligned}
$$

The unknown parameters in model (3.3) include $\boldsymbol{\theta} = (\eta, \beta_1, \phi_1, \rho, \varphi, d, \gamma_1, \ldots, \gamma_K)$. Con-

rad and Haag (2006) derived the nonnegativity conditions for the conditional variance in

the FIGARCH(p,d,q) model of the order $p \leq 2$ under a linear framework, while the sta-

tionarity condition for general FIGARCH process is still an open question. In our nonlinear

LFIGX$(1,d,1)$ model, the parameters do not need to satisfy any nonnegativity constraints

to make the model be well-defined.

The estimation for the fractionally integrated models necessitates the truncation of the infinite distributed lags in model (3.3). In the estimation, we consider the coefficients with the truncating R number of lag polynomial, that is

$$\psi_R(L) = 1 - \frac{(1 - \phi_1 L)(1 - L)^d}{1 - \beta_1 L} = \sum_{k=1}^{R} \psi_k L^k. \tag{3.4}$$

Because the fractional differencing operator is designed to model the long-memory features of the series, a too low truncation at a lag may loss important long-run dependencies information (Baillie et al., 1996). Our Covid-19 dataset has small sample size (around 700), so we set $R = 200$ as an illustration in real data analysis and investigate the effect of R in the numerical analysis.

3.2   Bayesian approach and parameter estimation

Bayesian methods have been increasingly applied to diverse research areas, which are considered as a staple in modern statistical analysis. We tackle the estimation problem only for LFIGX$(1, d, 1)$ model with the Bayesian method as an illustration. The Markov Chain Monte Carlo (MCMC) procedure is adopted to produce a powerful analysis for the proposed models, which is advantageous to incorporate the parameter constraints via a prior density.

For notational simplicity, let $\boldsymbol{\vartheta} = (\eta, \beta_1, \phi_1)$ and $\Gamma = (\gamma_1, \ldots, \gamma_K)$. Let $\boldsymbol{\theta}_\ell$ denotes certain parameter group in $\boldsymbol{\theta}$, i.e., $\boldsymbol{\vartheta}$, ρ, φ, d, and Γ, respectively for $\ell = 1, \cdots, 5$, and $\pi(\boldsymbol{\theta}_\ell)$ is its prior density. Let $\boldsymbol{\theta}_{\neq \ell}$ be the parameter vector of $\boldsymbol{\theta}$ excluding the element $\boldsymbol{\theta}_\ell$.

Given the series of counts $\mathbf{Y}_t$ up to time t and the covariates $\mathbf{X}_{t-1}$ up to time $t-1$, the

LFIGX$(1, d, 1)$ model (3.3) with parameter $\boldsymbol{\theta}$ has the conditional likelihood function:

$$L(\mathbf{Y}_t|\mathbf{X}_{t-1}, \boldsymbol{\vartheta}) = \Pi_{Y_s=0}\left\{\rho + (1-\rho)e^{-\lambda_s^*}\right\} \Pi_{Y_s>0}\left\{(1-\rho)\frac{\lambda_s^*(\lambda_s^* + \varphi Y_s)^{Y_s-1}}{Y_s!}e^{[-(\lambda_s^*+\varphi Y_s)]}\right\},$$
(3.5)

where λ_s^* is computed recursively by

$$\lambda_s^* = \frac{1-\varphi}{1-\rho}\exp\left(\eta + \psi_R(L)\log(Y_s+1) + \sum_{k=1}^{K}\gamma_k X_{s-1,k}\right), \text{ for } R \leq s \leq t.$$
(3.6)

To ensure the required constraints, for first group $\boldsymbol{\vartheta}$, since it is still an open question for

the stationarity conditions of $\boldsymbol{\vartheta}$, we consider setting restrictions to $\boldsymbol{\vartheta}$ such that all the roots

of $\Phi(L)$ and $1 - \beta(L)$ lie outside the unit circle. That is, $\phi_1 \in [-1, 1]$ while not equal to β_1,

and $\beta_1 \in [-1, 1]$. We adopt a constrained uniform prior defined by indicator $I(A_1)$, where

A_1 is the set of $\boldsymbol{\vartheta}$ satisfying the restrictions above. This uniform prior generates a flat

prior on the parameters in $\boldsymbol{\vartheta}$ restricted by the indicator that is non-zero inside A_1 and zero

outside. We also adopt constrained uniform priors on the parameters (groups) ρ, φ and d

defined by indicators $I(A_j)$, $j = 2, \ldots, 4$, where A_j is the set of corresponding parameter

satisfying $0 \leqslant \rho < 1$, $0 \leqslant \varphi < 1$, and $0 < d \leq 0.5$, respectively. We again adopt a flat prior

on the components of $\Gamma = (\gamma_1, \ldots, \gamma_K)$, denoted by $I(A_5)$. The choices of priors are similar

in Chen and Lee (2016) and Xu et al. (2020), which are not the only ones possible, but are

instead chosen to be non-informative.

We use the likelihood and the priors that were described above to give the conditional

posterior kernels for each parameter group as follows. For notational convenience, let f

denote the target density given by

$$p(\boldsymbol{\theta}_\ell|\mathbf{Y}_t, \mathbf{X}_{t-1}, \boldsymbol{\theta}_{\neq\ell}) \propto p(\mathbf{Y}_t|\mathbf{X}_{t-1}, \boldsymbol{\theta})\pi(\boldsymbol{\theta}_\ell|\boldsymbol{\theta}_{\neq\ell}),$$

$$\propto \Pi_{Y_s=0}\left\{\rho + (1-\rho)e^{-\lambda_s^*}\right\}\Pi_{Y_s>0}\left\{(1-\rho)\{\lambda_s^*(\lambda_s^* + \varphi Y_s)^{Y_s-1}\}e^{[-(\lambda_s^*+\varphi Y_s)]}\right\}I(A_\ell) \tag{3.7}$$

Details of the MH steps for $\boldsymbol{\theta}_\ell$ are as follows.

Step 1: At iteration i, generate a point $\boldsymbol{\theta}_\ell^* = \boldsymbol{\theta}_\ell^{[i-1]} + N(\mathbf{0}, c_\ell\Sigma_\ell)$, where c_ℓ is the scaling parameter of the normal proposal, which could be adjusted by controlling the acceptance rate of the posterior samples (Gelman et al., 1996), and Σ_ℓ is covariance matrix in the random walks of $\boldsymbol{\theta}_\ell$. The stability condition of $\boldsymbol{\theta}_\ell$ would be imposed through an accept-rejection MH sampling procedure.

Step 2: Accept $\boldsymbol{\theta}_\ell^*$ as $\boldsymbol{\theta}_\ell^{[i]}$ with probability

$$\min\left\{1, f(\boldsymbol{\theta}_\ell^*)/f(\boldsymbol{\theta}_\ell^{[i-1]})\right\},$$

where $\boldsymbol{\theta}_\ell^{[i]}$ is the ith iterate of $\boldsymbol{\theta}_\ell$. Otherwise, set $\boldsymbol{\theta}_\ell^{[i]} = \boldsymbol{\theta}_\ell^{[i-1]}$.

Usually a suitable value of c_ℓ with good convergence properties can be chosen by setting an acceptance probability of 25% to 50% (Chen and So, 2006).

Finally we construct the estimate of intensity λ_t from the mean of the posterior distribution via the MCMC sampling scheme by

$$\hat{\lambda}_t = \frac{1}{N-M}\sum_{i=M+1}^{N}\lambda_t^{[i]},$$

where $\lambda_t^{[i]}$ is the i-th iteration of λ_t recursively constructed using $\boldsymbol{\vartheta}^{[i]}$, $\rho^{[i]}$, $\varphi^{[i]}$, $d^{[i]}$, and $\Gamma^{[i]}$. N is the total number of iterates, and M is the number of burn-in iterates. In the following sections we set $N = 15,000$ for the simulation study and $N = 20,000$ for real data analysis. We drop the first $M = 3000$ iterations as a burn-in sample.

4. Simulation

In this section, we examine the finite-sample performance of the LFIGX model. We investigate the estimation performance and compare it with several alternative models under different data generating processes. Moreover, we conduct robustness analysis on the choice of priors in the MCMC procedure, the effect of truncating number R of the lag polynomial, and the estimation performance under misspecified number of the exogenous variables. Source code for simulation replication and reproducibility is available online at `https://github.com/Xiaofei-Xu/LFIGX-project`.

4.1 Estimation analysis

In this section, we examine the performance of the LFIGX model in inference under a known data generating process with two exogenous covariates. We also provide a detailed comparison with several alternative methods.

To investigate the estimation performance, we generate count series in a homogeneous scenario with a set of globally constant parameters. We consider three scenarios for data generation: LFIGX$(1, d, 1)$ (denoted as DS-default), LFIG$(1, d, 1)$ (i.e., without exogenous covariates, denoted as DS-X), and LFIGX$(0, d, 1)$ (i.e., $\phi_1 = 0$, denoted as DS-ϕ). We use

sample sizes of $n = 400$, 900, and 1300, and start the estimation from time $t = 201$, 601, and 1001, respectively, until the end for each scenario. For $n = 400$, we set $R = 200$ to mimic the real data situation with small sample size and R value. For $n = 900$ and 1300, we set $R = 600$ and 1000, respectively, considering the larger sample size. The parameter sets of $\boldsymbol{\theta}$ in each design are reported in Table 2. We generate a total of 200 replications for each design. The two exogenous covariates, x_1 and x_2, are generated from the standard normal distribution.

Table 2: Estimation and corresponding standard deviation (in parentheses) of the parameters using LFIGX modelling under $n = 400$. The in-sample log-likelihood, AIC, and BIC are also reported.

Scenario		LogLik	AIC	BIC	η	ϕ_1	β_1	ρ	φ	d	γ_1	γ_2
True value					0.600	0.700	0.400	0.200	0.400	0.200	0.500	-0.300
	$d = 0.1$	-586.75	1215.88	1189.50	0.732	0.745	0.349	0.204	0.396	0.100	0.500	-0.297
					(0.086)	(0.040)	(0.054)	(0.031)	(0.038)		(0.028)	(0.033)
	$d = 0.2$	**-586.51**	**1215.40**	**1189.01**	**0.602**	**0.683**	**0.384**	**0.204**	**0.395**	**0.200**	**0.500**	**-0.297**
					(0.068)	(0.054)	(0.066)	(0.031)	(0.037)		(0.028)	(0.033)
DS-default	$d = 0.3$	-587.15	1216.68	1190.29	0.495	0.604	0.399	0.203	0.396	0.300	0.501	-0.297
					(0.057)	(0.080)	(0.089)	(0.031)	(0.037)		(0.029)	(0.034)
	$d = 0.4$	-589.21	1220.81	1194.43	0.414	0.420	0.308	0.202	0.403	0.400	0.501	-0.297
					(0.049)	(0.160)	(0.154)	(0.032)	(0.038)		(0.031)	(0.036)
	$d = 0.5$	-592.00	1226.39	1200.00	0.340	0.102	0.092	0.200	0.408	0.500	0.503	-0.298
					(0.045)	(0.233)	(0.226)	(0.032)	(0.040)		(0.033)	(0.037)
True value					0.600	0.700	0.400	0.200	0.400	0.200	0.000	0.000
	$d = 0.1$	-587.41	1217.20	1190.81	0.721	0.743	0.342	0.204	0.394	0.100	-0.001	-0.002
					(0.090)	(0.045)	(0.069)	(0.030)	(0.039)		(0.030)	(0.035)
	$d = 0.2$	**-587.37**	**1217.12**	**1190.74**	**0.595**	**0.677**	**0.371**	**0.204**	**0.394**	**0.200**	**-0.001**	**-0.003**
					(0.071)	(0.063)	(0.081)	(0.030)	(0.039)		(0.030)	(0.035)
DS-X	$d = 0.3$	-588.50	1219.38	1192.99	0.491	0.587	0.373	0.202	0.397	0.300	-0.001	-0.002
					(0.059)	(0.104)	(0.115)	(0.030)	(0.039)		(0.030)	(0.036)
	$d = 0.4$	-589.96	1222.30	1195.91	0.412	0.389	0.267	0.201	0.401	0.400	-0.002	-0.003
					(0.051)	(0.171)	(0.163)	(0.031)	(0.038)		(0.031)	(0.037)
	$d = 0.5$	-591.64	1225.67	1199.28	0.342	0.097	0.074	0.199	0.404	0.500	-0.002	-0.003
					(0.044)	(0.221)	(0.212)	(0.030)	(0.038)		(0.032)	(0.038)
True value					0.600	0.000	0.400	0.200	0.400	0.200	0.500	-0.300
	$d = 0.1$	-453.98	950.35	923.96	0.930	-0.081	0.221	0.194	0.393	0.100	0.493	-0.295
					(0.122)	(0.153)	(0.145)	(0.040)	(0.048)		(0.061)	(0.067)
	$d = 0.2$	**-453.84**	**950.07**	**923.68**	**0.605**	**-0.022**	**0.379**	**0.195**	**0.393**	**0.200**	**0.494**	**-0.296**
					(0.104)	(0.144)	(0.130)	(0.039)	(0.049)		(0.060)	(0.068)
DS-ϕ	$d = 0.3$	-454.06	950.50	924.12	0.397	0.012	0.509	0.195	0.393	0.300	0.495	-0.296
					(0.091)	(0.134)	(0.112)	(0.039)	(0.048)		(0.061)	(0.067)
	$d = 0.4$	-454.50	951.39	925.00	0.258	0.018	0.608	0.194	0.395	0.400	0.495	-0.295
					(0.079)	(0.118)	(0.095)	(0.039)	(0.047)		(0.061)	(0.068)
	$d = 0.5$	-454.94	952.28	925.89	0.168	0.008	0.694	0.193	0.397	0.500	0.495	-0.296
					(0.069)	(0.102)	(0.077)	(0.039)	(0.047)		(0.061)	(0.069)

The row labeled by "True value" indicates the true value of parameters in each design. Each experiment is replicated 200 times. The best performance is marked in bold.

Table 2 reports the parameter estimation and standard deviations for the three scenarios with $n = 400$. Since we find that direct estimation of the parameter d poses a challenge, hence, we suggest selecting the value of d based on the likelihood results of a few candidates, and we also compute the AIC and BIC results with d varying for d estimation. To achieve this, we obtained five sets of parameter estimates while keeping d fixed at 0.1, 0.2, 0.3, 0.4, and 0.5, respectively. The results reveal that the correct guess, $d = 0.2$, yields the best fitting results of likelihood, AIC and BIC(rows with bold values), as expected, across all three designs. For each design, the parameter estimates are quite accurate where the estimated coefficients are close to the true value, with relatively small standard deviations as well, under the correct estimated value of d. This reflects that it is feasible to conduct estimation of d with likelihood and AIC/BIC and the Bayesian estimation provides reasonable estimates of parameters in LFIGX modeling.

Table 3 reports the estimated parameters and their standard deviations for the three scenarios with sample sizes of 900 and 1300. We only present the results with fixed $d = 0.2$ which is selected with maximum likelihood value among five candidates. It shows that the LFIGX model exhibits accurate and stable estimation among different data generation processes and sample sizes, with the estimated parameters close to the true values for each case, and the standard deviations of almost all parameters are relatively small and decrease as the sample size increases.

To compare estimation accuracy, we consider four prevalent short memory models over the same estimation period: the P-INGARCH, log-linear GP-INGARCHX, log-linear ZIGP-INGARCH, and log-linear ZIGP-INGARCHX models. The P-INGARCH model

Table 3: Estimation and corresponding standard deviation (SD) of the parameters using LFIGX modeling under $n = 900$ and 1300. The symbol "$-$" refers that $d = 0.2$ is fixed during estimation.

Scenario		η	ϕ_1	β_1	ρ	φ	d	γ_1	γ_2
					$n = 900$				
DS-default	True	0.600	0.700	0.400	0.200	0.400	0.200	0.500	-0.300
	Estimate	0.597	0.696	0.398	0.203	0.405	$-$	0.499	-0.302
	SD	(0.051)	(0.032)	(0.043)	(0.026)	(0.031)	$-$	(0.020)	(0.022)
DS-X	True	0.600	0.700	0.400	0.200	0.400	0.200	0.000	0.000
	Estimate	0.594	0.692	0.388	0.202	0.395	$-$	0.001	0.000
	SD	(0.056)	(0.045)	(0.057)	(0.024)	(0.030)	$-$	(0.024)	(0.024)
DS-ϕ	True	0.600	0.000	0.400	0.200	0.400	0.200	0.500	-0.300
	Estimate	0.596	0.003	0.398	0.202	0.401	$-$	0.498	-0.304
	SD	(0.070)	(0.107)	(0.091)	(0.029)	(0.034)	$-$	(0.046)	(0.041)
					$n = 1300$				
DS-default	True	0.600	0.700	0.400	0.200	0.400	0.200	0.500	-0.300
	Estimate	0.597	0.695	0.395	0.202	0.399	$-$	0.500	-0.300
	SD	(0.047)	(0.035)	(0.045)	(0.024)	(0.028)	$-$	(0.020)	(0.020)
DS-X	True	0.600	0.700	0.400	0.200	0.400	0.200	0.000	0.000
	Estimate	0.596	0.695	0.397	0.203	0.397	$-$	-0.002	0.002
	SD	(0.054)	(0.042)	(0.055)	(0.024)	(0.034)	$-$	(0.022)	(0.024)
DS-ϕ	True	0.600	0.000	0.400	0.200	0.400	0.200	0.500	-0.300
	Estimate	0.595	-0.021	0.379	0.197	0.397	$-$	0.498	-0.302
	SD	(0.067)	(0.099)	(0.086)	(0.028)	(0.036)	$-$	(0.046)	(0.041)

(Ferland et al., 2006) is widely used for count time series with overdispersion. The log-linear GP-INGARCHX (Chen and Lee, 2017) is also a popular count time modeling which could account for both overdispersion and underdispersion and also enable to include exogenous covariates in a straightforward manner. The other two models have been well studied for the log-linear zero-inflated over-dispersed counts with/without the effect of exogenous covariates (Lee et al., 2016; Xu et al., 2020). Table 4 summarizes the root mean squared error (RMSE) and mean absolute deviation (MAD) of the estimated intensity λ_t of the five models. The LFIGX model outperforms the other four short memory models with better accuracy in terms of RMSE and MAD by accounting for the long-range dependence involved in the count time series.

Table 4: RMSE and MAD of the λ_t estimation of three designs using LFIGX model compared with P-INGARCH, GP-INGARCHX, ZIGP-INGARCH, ZIGP-INGARCHX models under different sample sizes. The best accuracy is highlighted in bold.

Model	P-INGARCH		GP-INGARCHX		ZIGP-INGARCH		ZIGP-INGARCHX		LFIGX	
n=400	RMSE	MAD	RMSE	MAD	RMSE	MAD	RMSE	MAD	RMSE	MAD
DS-default	16.771	9.056	13.805	7.830	15.773	8.719	4.846	2.603	**1.925**	**1.052**
DS-X	2.103	1.438	5.512	4.042	1.349	0.952	1.462	0.997	**1.228**	**0.859**
DS-ϕ	2.754	1.980	1.095	0.716	2.747	1.963	0.847	0.559	**0.666**	**0.447**
n=900										
DS-default	23.962	11.889	26.689	17.465	22.437	11.488	6.962	3.383	**0.741**	**0.385**
DS-X	2.562	1.702	9.461	8.544	1.510	1.044	1.608	1.071	**1.188**	**0.813**
DS-ϕ	4.521	4.322	1.582	1.250	3.371	2.383	0.917	0.603	**0.593**	**0.387**
n=1300										
DS-default	25.557	12.993	23.750	13.122	23.887	12.533	7.333	3.673	**2.032**	**1.063**
DS-X	2.827	1.873	8.979	6.605	1.716	1.184	1.727	1.144	**1.300**	**0.886**
DS-ϕ	3.751	2.694	1.417	0.935	3.742	2.682	0.982	0.650	**0.629**	**0.419**

4.2   Robustness checking

We investigate the sensitivity of the LFIGX model to various hyperparameters, including the choice of priors in the MCMC procedure, truncating value R. We also study the effect of misspecified exogenous covariates as pointed by one referee. To demonstrate the robustness of the model, we consider the design DS-default with $(\eta, \phi_1, \beta_1, \rho, \varphi, d, \gamma_1, \gamma_2)$=(0.6, 0.7, 0.4, 0.2, 0.4, 0.2, 0.5, -0.3), $R = 600$, and $n = 900$. For each robustness experiment, we apply alternative priors, R, and different exogenous covariates, redo the estimation, and compare the estimation performance with the default setup.

We begin by exploring the impact of different priors on the MCMC sampling procedure. The default choice is non-informative (uniform/flat) priors for all parameters, but this is not the only possibility. As an illustration, we consider setting the beta distribution as the priors for parameter ρ and φ (Chen and Lee, 2016), and the normal distribution for Γ. In specific, the following priors are applied: Prior 1: $\rho \sim \text{Beta}(2, 8)$, $\varphi \sim \text{Uniform}(0,1)$, $\gamma_k \sim N(0, 0.5), k = 1, 2$; Prior 2: $\rho \sim \text{Beta}(10, 90)$, $\varphi \sim \text{Beta}(6, 4)$, $\gamma_k \sim N(0, 0.5), k = 1, 2$;

Prior 3: $\rho \sim \text{Uniform}(0,1)$, $\varphi \sim \text{Beta}(60, 40)$, $\gamma_k \sim N(0, 0.5)$, $k = 1, 2$. We conduct estimation for the DS-default design using these alternative priors and compare their estimation performance.

As the fractional differencing operator $\psi(L)$ is designed to capture the long-memory features of the process, truncating at a too low lag may result in the loss of important long-run dependencies. In the DS-default design, the process is restricted with $R = 600$. To examine the sensitivity of the estimation results to the truncating value, we consider two alternative settings with $R = 200$ and $R = 700$, denoted as "R1" and "R2", respectively. Lastly, we investigate the impact of effective covariates by conducting a robustness check on misspecified models by missing effective covariates or including unrelated covariates in the model. In each robustness experiment, we keep all remaining settings the same as in the default case, except for the hyper-parameters under investigation.

Table 5: Robustness checking.

	η	ϕ_1	β_1	ρ	φ	d	γ_1	γ_2	γ_3	Loglik	AIC	BIC
True	0.6	0.7	0.4	0.2	0.4	0.2	0.5	-0.3	0.0			
Default	0.597	0.696	0.398	0.203	0.405	0.200	0.499	-0.302	−	-914.009	1873.648	1844.018
Prior1	0.599	0.696	0.398	0.201	0.404	0.200	0.499	-0.302	−	-913.996	1873.622	1843.992
Prior2	0.631	0.696	0.397	0.174	0.413	0.200	0.499	-0.302	−	-914.823	1875.277	1845.646
Prior3	0.611	0.691	0.395	0.202	0.459	0.200	0.497	-0.301	−	-914.796	1875.222	1845.592
R1	0.669	0.697	0.399	0.201	0.405	0.200	0.496	-0.298	−	-916.311	1878.252	1848.622
R2	0.583	0.693	0.392	0.204	0.402	0.200	0.505	-0.302	−	-908.221	1862.073	1832.443
3X	0.597	0.696	0.399	0.204	0.404	0.200	0.498	-0.302	-0.006	-913.458	1878.251	1844.917
1X	0.717	0.658	0.381	0.195	0.595	0.200	0.479	−	−	-987.382	2014.691	1988.765

"Default" refers to the results under default setup. "Prior1" − "Prior3" refer to the results under 3 alternative priors. "R1" and "R2" refer to two different truncating number $R = 200$ and 700 in the estimation, respectively. "3X" and "1X" refers to the misspecified model with one additional covariate or only with the first covariate, respectively. The symbol "−" means the model/estimation does not involve this parameter.

Table 5 reports the robustness checking results under alternative priors, R values, and misspecified models (wrong exogenous covariates). It shows that the parameter estimation

is not sensitive to the selection of priors (ρ, φ, Γ) by delivering similar results to the default.

Regarding the choice of R, as stated before, using a too small value may lead in information

loss, it does induce some bias in the parameter estimation, especailly for η, while the other

parameters seem to be less affected. The results are consistent to the experiments results in

Segnon and Stapper (2019) for R's influence study. The improvement of estimation is not

significant by using a larger value of R. Lastly, adding unrelated covariates to the model

does not cause any issues for the estimation of other parameters, where the estimated

coefficient of the unrelated covariates is almost zero. While when some of the effective

covariates are missing, there exists influence in parameter estimation, especially for η and

over-dispersion parameter φ, while notably, there is no significant effect for the estimating

of γ_1, the coefficient of the remaining covariate, though missing certain effective covariates.

In summary, the simulation study shows stable and accurate performances of the LFIGX

model under different scenarios with accurate estimation of parameters with truly selected

d. The adaptive Bayesian estimation is robust to the choice of priors. A too small value

of R does show some influence in parameter estimation, especially for η, and larger value

of R has little improvement in estimation accuracy. Excluding some covariates leads to

variations in the estimates of η, while the estimation of the coefficients for the remaining

covariates is still stable and accurate.

5.   Real Data Analysis

In this section, we apply the LFIGX$(1, d, 1)$ model to investigate the dynamic evolution

of the daily new Covid-19 case time series of the six countries. We initialize the first 500

observations for in-sample analysis and conduct the forecasting from the 501th day till the ending of each dataset. The exogenous covariates X_t includes 3 variables: policy index, temperature, and a weekend dummy. The detailed description of datasets is in Section 2.

5.1   Interpretation

We investigate the long memory property and the effect of exogenous covariates through the in-sample analysis using the proposed LFIGX$(1, d, 1)$ model. To evaluate the immediate- and longer-period effect of the policy after its implementation, we consider using the lag$-h$ policy index variable, denoted as Policy$_{t-h}$, and the lag$-h$ temperature variable, denoted by Temperature$_{t-h}$, while the weekend dummy variable at current time, i.e. D_t, is used since D_t is always available according to the Gregorian calendar. The model is as follows.

$$Y_t|(F_{t-1}^{(y)}, \tilde{\mathbf{X}}_{t-h}) \sim \text{ZIGP}(\lambda_t^*, \varphi, \rho),$$
$$\lambda_t^* = \frac{1-\varphi}{1-\rho}\lambda_t, \ \log(\lambda_t) = \eta + \psi_R(L)\log(Y_t+1) + \gamma_1\text{Policy}_{t-h} + \gamma_2\text{Temperature}_{t-h} + \gamma_3 D_t,$$

$$(5.8)$$

where $\tilde{\mathbf{X}}_{t-h}$ is the σ-field generated by $\{\text{Policy}_{t-h}, \ldots, \text{Policy}_1, \text{Temperature}_{t-h}, \ldots,$ Temperature$_1, D_t, \ldots, D_1\}$ representing all available past information of exogenous variables policy and temperature till time $t - h$, and weekend dummy variable till time t. We consider $h = 1, 2, 7$, and 14 in the empirical study to evaluate the immediate policy impact in the following one and two days after implementation, and middle-term delayed effect after 1 and 2 weeks of implementation.

Table 6 reports the estimated parameters of the LFIGX$(1, d, 1)$ model using the first 500 observations with $R = 200$ under $h = 1$ for Policy$_{t-h}$ and Temperature$_{t-h}$. The LFIGX

model delivers different features of the daily new Covid-19 cases among six countries with different levels of persistence, dependence, and impact of exogenous variables. For example, the coefficient ϕ_1 is 0.916 and 0.708 for ITA and GBR, respectively, and the magnitude is much stronger than other countries, indicting a significant and positive neighborhood effect for the two European countries, while the effect is weaker for the Asian and American countries. It also shows that the daily new cases series is likely to be modeled by a long-memory process with nonzero estimate of d. For ITA, $d = 0.0144$ which is smallest among the six countries, indicating moderate persistence in the count process. This is consistent to the feature displayed in Figure 2 where the ACF of ITA decays fast and becomes insignificant after lag order of 40. For JPN and VNM, $d = 0.482$ and 0.446, respectively, indicating higher persistence in Covid-19 count series at these two Asian countries. For the ZIGP distribution variables, the over-dispersion parameter φ is greater than 0.8 for all counties which is consistent to the significant over-dispersion feature of the series. The zero-inflation parameter ρ is smaller than 0.1, which is also consistent to the fact that zero percentage is quite low for all the datasets except for VNM.

Table 6: The estimates of the parameters in LFIGX$(1, d, 1)$ model using the first 500 observations. The estimated coefficients are obtained using the model with $h = 1$ for Policy$_{t-h}$ and Temperature$_{t-h}$.

Country	η	ϕ_1	β_1	ρ	ϕ	d	Policy (γ_1)	Temp. (γ_2)	W.D. (γ_3)
JPN	1.098	0.275	-0.130	0.004	0.909	0.482	-0.014	-0.002	-0.194
VNM	0.930	-0.287	-0.022	0.010	0.804	0.446	0.001	-0.002	-0.076
ITA	1.108	0.916	0.361	0.026	0.958	0.144	-0.008	0.001	-0.063
GBR	0.739	0.708	-0.065	0.009	0.956	0.267	-0.001	-0.001	-0.134
USA	0.841	0.459	-0.009	0.006	0.986	0.315	0.002	0.000	-0.124
BRA	0.157	-0.115	-0.530	0.021	0.985	0.303	0.006	0.010	-0.118

The long memory dependence of Covid-19 pandemic could be caused by the effect of

exogenous variables such as policy and temperature, which could affect the latent intensity

process λ_t in a long-range pattern. Figure 4 displays the estimated coefficients and corre-

sponding 95% credible intervals for policy index and temperature with $h = 1, 2, 7$ and 14

respectively. It shows that the policy effect changes with different time period after policy

implementation. There is only weak immediate policy impact with small magnitude of

coefficient at $h = 1$, while it presents a stronger negative intermediate impact after 7 and

14 days with much greater magnitude. For example, when $h = 1$, the coefficient of policy

is close to zero for all countries except JPN, while when h increases to 14, the negative

coefficient's magnitude becomes larger for all countries except USA, which means that the

policy effect becomes more significant after 2 weeks' introduction. The findings indicate

that there exists a delay in the impact of policy after implementation, it is hard to obtain

immediate policy impact, while the policy impact in reducing the daily new Covid-19 cases

becomes more significant after 2 weeks.

Temperature shows positive effect with a stronger magnitude when h is larger, indicating

that after a longer period of policy introduction (14 days), a higher level of the daily new

cases of Covid-19 is likely to occur as a result of warmer temperatures. While if a strict

policy is implemented at previous day, the hot temperature effect to new cases at following

two days is less significant. For example, for the two European countries, the immediate

temperature effect (i.e. $h = 1$) is 0.001 and -0.001 in ITA and GBR, respectively, while the

impact increases to 0.009 and 0.030, respectively when $h = 14$. This is possibly due to the

fact that after observing a drop of the daily new cases and after a certain period time of

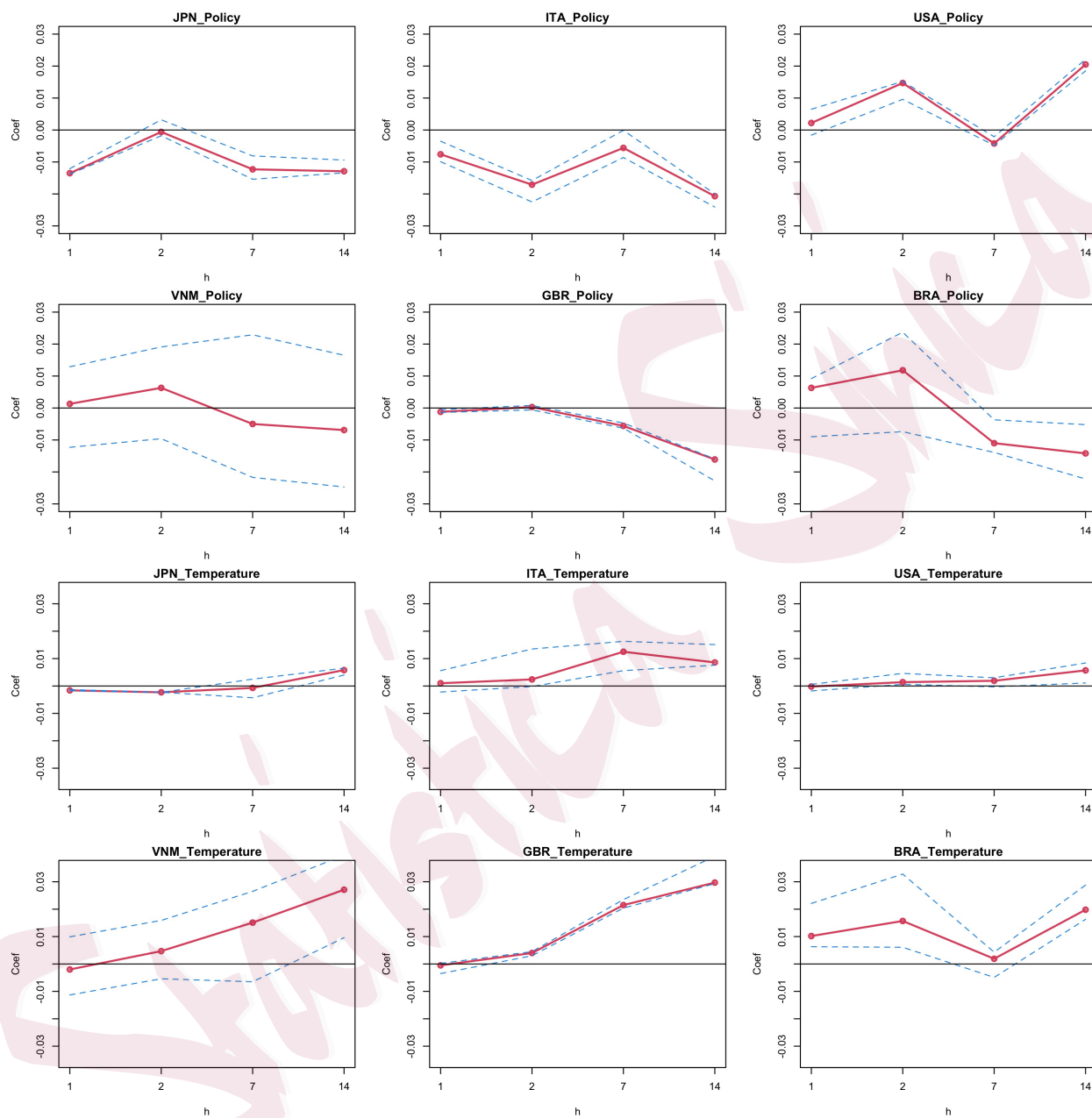strict policy introduction, e.g., two weeks, people may get tired of tight regulations and start

Figure 4: The estimated coefficients for policy index (top two rows) and temperature variable (bottom two rows) with $h = 1, 2, 7$ and 14 for the six countries. The solid line is the estimated parameter and dashed lines refer to the corresponding 95% credible interval.

to increase social activity and retaliatory gathering under warm weather, which, in turn, could expand the possibility of infection. This result is consistent with Han et al. (2022) and Qiu et al. (2020), who documented that cold weather tends to discourage social activity

and decrease Covid-19 virus transmission. The feature of warm temperature effect is more obvious for ITA, GBR and VNM than JPN and USA. Moreover, there exhibits negative coefficient for the weekend dummy variable, indicting smaller new cases at weekend than weekdays. While this is possibly because of the test number difference at a weekday and weekend.

5.2   Out-of-sample forecasting

We conduct a set of multi-period ahead forecasting experiments to the daily new Covid-19 cases of the six countries. In addition to the conventional $1-$day ahead forecasts, we consider $h = 2$, 7 and 14, covering $1-$ and $2-$day, $1-$ and $2-$week ahead forecasts. We start the forecasting from the 501th observation to the end of each dataset. The ZIGP-INGARCH(1,1) model is considered as a comparative short memory model.

We directly predict counts at time $t + h$ with the observations at time t, which is more robust than the iterated forecast under model misspecification (Marcellino et al., 2006). Especially, we compute the h-day ahead forecast as follows.

$$Y_{t+h}|(F_t^{(y)}, \tilde{\mathbf{X}}_t) \sim \text{ZIGP}(\lambda_{t+h}^*, \varphi_{t+h}, \rho_{t+h}),$$

$$\lambda_{t+h}^* = \frac{1 - \varphi_{t+h}}{1 - \rho_{t+h}}\lambda_{t+h},$$

$$\log(\lambda_{t+h}) = \eta_t + \sum_{k=0}^{R} \psi_{k,t}L^k \log(Y_t + 1) + \gamma_1\text{Policy}_t + \gamma_2\text{Temperature}_t + \gamma_3 D_{t+h},$$

where the definition of $\tilde{\mathbf{X}}_t$ is similar as (5.8). Since the daily new cases of Covid-19 exhibit non-stationary pattern, at each time point t, instead of using all the past observations to

conduct Bayesian estimation, we apply rolling window technique using subsamples within the interval $I_t = [t - m, t]$ for parameter estimation. We consider a rolling window size of $m = 30$ days. That is, we move forward one day at a time to re-do the estimation using the past 30 days data up to that point and conduct forecast until reaching the end of the sample.

As the intensity λ_t is the conditional expectation of observed counts which represents the essential feature of the data, we thus consider evaluating the prediction performance by the mean squared error (MSE) of the Pearson residuals defined by

$$\text{MSE} = \frac{1}{T - t_0 - h} \sum_{t=t_0+1}^{T-h} \left(\frac{Y_{t+h} - \hat{\lambda}_{t+h}}{\sqrt{\text{Var}(Y_{t+h}|(F_t^{(y)}, \tilde{\mathbf{X}}_t)}} \right)^2,$$

where $t_0 + 1$ indicates the starting time point of forecasting.

Table 7 reports the MSE using the LFIGX$(1, d, 1)$ model and the ZIGP-INGARCH$(1,1)$ model for out-of-sample h-day ahead forecasting of the six datasets. It shows that LFIGX model presents better forecasting performance with smaller MSE than short memory ZIGP-INGARCH$(1,1)$ model among various forecasting horizons and countries. For example, when $h = 1$, the LFIGX model outperforms the ZIGP-INGARCH$(1,1)$ at all countries with smaller MSE. For $h = 2$, 7, and 14, the LFIGX is also better than short memory model at 5 out 6 countries.

As illustration, Figures 5-7 display the h-day ahead forecasting with $h = 1$, 2, 7 and 14 using the LFIGX$(1, d, 1)$ model for JPN, GBR and BRA, respectively. See Figures B, C and D in the Supplementary Material for the results of VNM, ITA, and USA, respectively. For short period ahead forecasts at $h = 1$ and 2, the LFIGX$(1, d, 1)$ model delivers accurate

Table 7: The MSE of forecasting using the LFIGX$(1, d, 1)$ and the ZIGP-INGARCH(1,1) model with rolling window size of 30. The best forecast is marked in boldface.

Model	JPN	VNM	ITA	GBR	BRA	USA
$h = 1$						
LFIGX$(1, d, 1)$	**2.402**	**2.929**	**3.034**	**0.443**	**11.033**	**3.849**
ZIGP-INGARCH(1,1)	2.575	3.879	3.513	0.608	14.887	5.512
$h = 2$						
LFIGX$(1, d, 1)$	**6.370**	**3.442**	6.981	**0.819**	**8.970**	**4.971**
ZIGP-INGARCH(1,1)	7.616	4.440	**6.743**	1.021	14.158	8.126
$h = 7$						
LFIGX$(1, d, 1)$	**54.183**	**8.088**	**8.010**	**2.328**	**5.255**	3.962
ZIGP-INGARCH(1,1)	103.572	11.970	18.600	2.780	5.745	**3.564**
$h = 14$						
LFIGX$(1, d, 1)$	**394.593**	**43.314**	**53.047**	5.602	**15.446**	**2.705**
ZIGP-INGARCH(1,1)	592.102	72.805	53.380	**5.176**	16.102	2.850

forecasting performance to all datasets, although the forecast gets worse slightly along with the forecast horizons. The forecast of intensity process λ_t enables us to capture the dynamics of the daily new cases of Covid-19 series very well, and it presents a narrow 95% credible interval for the prediction, indicating that forecasting is not very dispersed but does exhibit dynamic changes. Even for the longer period forecasts of $h = 7$ and 14 days, the LFIGX$(1, d, 1)$ model still captures the dynamics of daily new cases series well with good prediction in GBR and BRA. For JPN, the LFIGX$(1, d, 1)$ is also able to capture the true dynamic pattern in general, while exhibiting certain delay in the prediction of the wave peak at around August-September 2021. It is not surprised that 14-days ahead forecast is worse than shorter horizons given the non-stationarity of datasets and the larger difficulty in long period ahead forecasting.
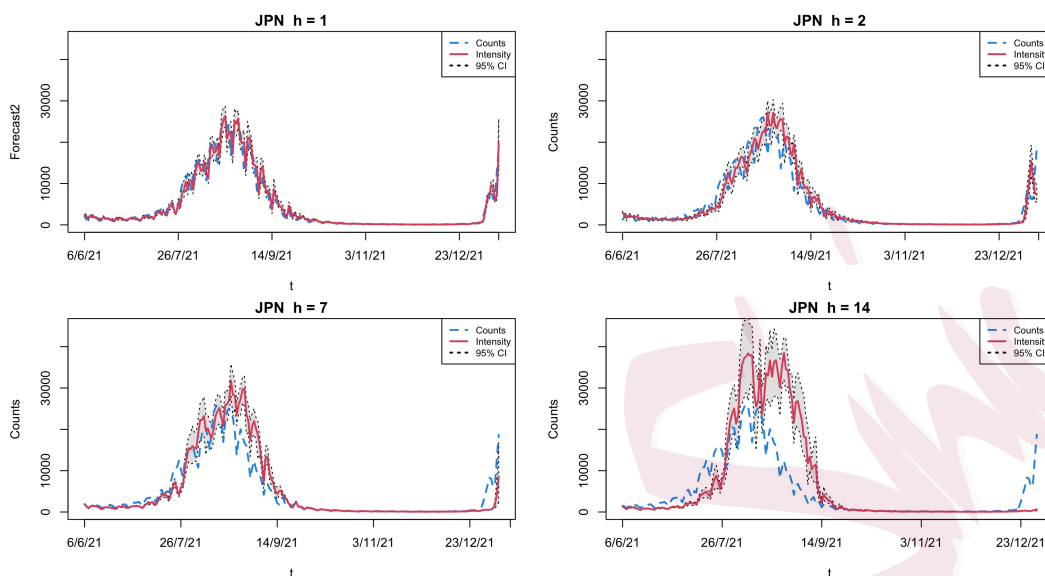
Figure 5: The h-day ahead forecasting using the LFIGX$(1, d, 1)$ model with $h =$1, 2, 7 and 14 for JPN.
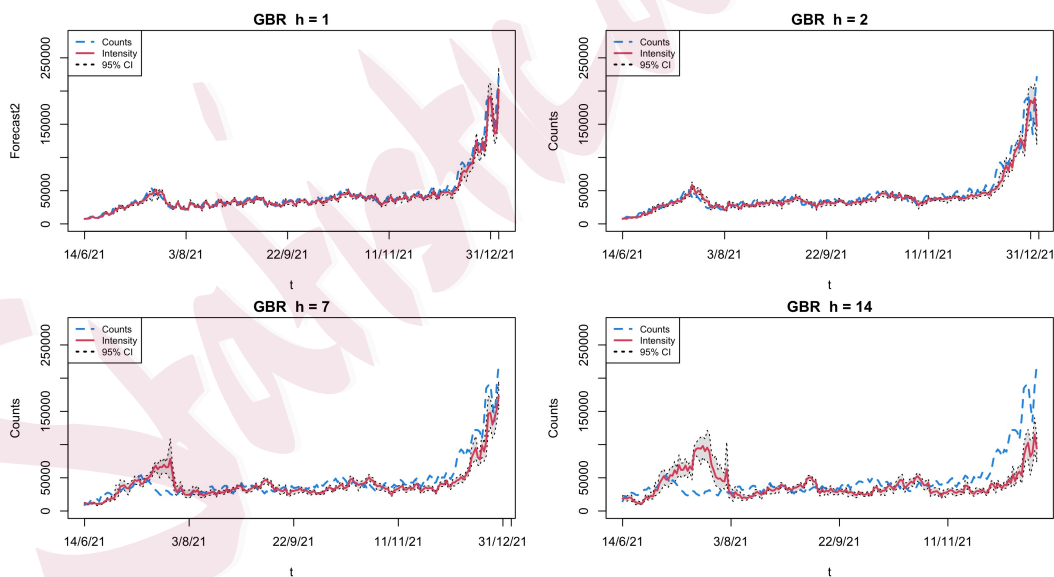

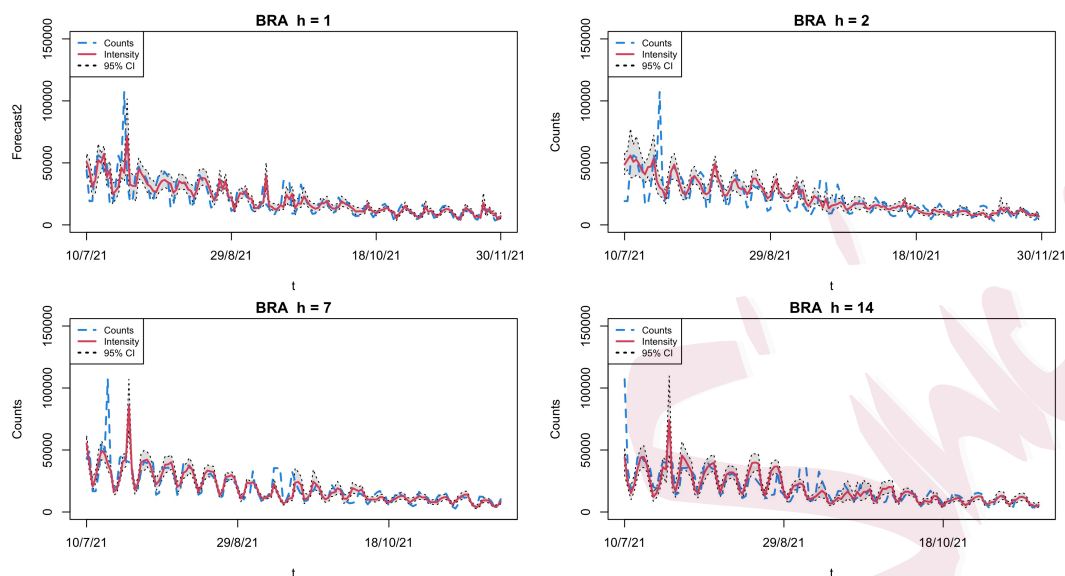Figure 6: The h-day ahead forecasting using the LFIGX$(1, d, 1)$ model with $h =$1, 2, 7 and 14 for GBR.

Figure 7: The h-day ahead forecasting using the LFIGX$(1, d, 1)$ model with $h =$1, 2, 7 and 14 for BRA.

6. Conclusion

In this paper, the LFIGX model (log-linear zero-inflated generalized Poisson integer-valued fractionally integrated GARCH model with exogenous covariates) is proposed for modeling the dynamics of the daily new Covid-19 cases. It is a novel long memory integer-valued modeling which accounts for multiple features including serial dependence (positive or negative), over-dispersion, zero-inflation, nonlinearity, and the effect of exogenous covariates in a unified framework. The parameters are estimated by an adaptive Bayesian Markov Chain Monte Carlo (MCMC) sampling scheme, which is quite new in the literature of long memory modeling to count time series. The LFIGX model delivers good interpretation and forecasting performance to the daily new Covid-19 cases for six countries across four continents: JPN, VNM, ITA, GBR, BRA and USA. We find that the effects of policies and temperature vary depending on the time period following their implementation. We

observe a weak immediate policy impact (e.g. 1 and 2 days), but a strong negative intermediate impact (e.g. 14 days) after policy implementation. Furthermore, we find that higher-level daily new Covid-19 cases tend to occur as a result of warmer temperatures after 14-days of policy introduction. This is possibly due to increased social activities in warm weather and a decrease in compliance with strict regulations after a certain period of policy introduction. For out-of-sample forecasting, the LFIGX model also delivers better forecasting accuracy than the comparative short memory model for most countries and forecast horizons.

Several extensions could be considered as future research. Firstly, it would be beneficial to investigate the theoretical properties for parameter estimation such as MCMC convergence rate and the central limit theorem of the LFIGX estimator. Liu (2001) provided a good review of theoretical study for Bayesian based MCMC technique. The theoretical derivation of Bayesian method in the long memory model would be an exciting direction for the count time series. It is also interesting to extend the LFIGX model to a multivariate framework for modeling multiple or even high-dimensional count time series simultaneously, or adopting spatial temporal models cooperated with long memory structure for Covid-19 data study, given that the change of policy or the new cases in one country may affect the Covid situation in other countries. This could possibly deliver new findings to capture principal features in the dynamics and effects of exogenous covariates on Covid-19. The multivariate INGARCH-models have been studied by Fokianos et al. (2020) and Cui et al. (2020). Han et al. (2022) and Celani and Giudici (2022) investigated the policy effectiveness on the Covid-19 pandemic by means of a spatio-temporal approach, allowing for

spatial and serial dependence. While there are few studies on the extension of these types of models to count time series in a long memory framework. Lastly, the proposed model provides a novel approach to handle multiple features, especially the long-range dependence phenomenon, in count time series. However, it is worth noting that the underlying source of long memory in the daily new cases of Covid-19 series still requires further investigation. In practice, dominant, universal and core factors such as policies, temperature, vaccines, and variants of Covid-19 virus could contribute to the long-range patterns of the latent intensity process. Additionally, different waves of the pandemic occur as clusters could be another possible cause of slowly decaying autocorrelation, as suggested by one referee. Exploring the essential cause of long-range dependence phenomenon and considering dynamic non-stationary models with time-varying parameters for infectious disease analysis could be promising avenues for further research on the study of Covid-19 data.

Supplementary Materials

The online supplementary materials provide some additional figures for the exogenous variables and forecasting performance of the LFIGX model in real data analysis as well as some empirical results of state-level study of USA considering the large land area of this country.

Acknowledgements

References

Agosto, A., A. Campmas, P. Giudici, and A. Renda (2021). Monitoring COVID-19 contagion growth. *Statistics in Medicine 40*(18), 4150–4160.

Atkeson, A. (2020). What will be the economic impact of COVID-19 in the US? rough estimates of disease scenarios. Technical report, National Bureau of Economic Research.

Baillie, R. T., T. Bollerslev, and H. O. Mikkelsen (1996). Fractionally integrated generalized autoregressive conditional heteroskedasticity. *Journal of Econometrics 74*(1), 3–30.

Bhardwaj, G. and N. R. Swanson (2006). An empirical investigation of the usefulness of ARFIMA models for predicting macroeconomic and financial time series. *Journal of Econometrics 131*(1-2), 539–578.

Bollerslev, T. and H. O. Mikkelsen (1996). Modeling and pricing long memory in stock market volatility. *Journal of Econometrics 73*(1), 151–184.

Celani, A. and P. Giudici (2022). Endemic-epidemic models to understand COVID-19 spatio-temporal evolution.

Spatial Statistics 49, 100528.

Chakraborty, I. and P. Maity (2020). COVID-19 outbreak: Migration, effects on society, global environment and prevention. *Science of the Total Environment 728*, 138882.

Chen, C. W. and S. Lee (2016). Generalized Poisson autoregressive models for time series of counts. *Computational Statistics & Data Analysis 99*, 51–67.

Chen, C. W., S. Lee, M. C. Dong, and M. Taniguchi (2021). What factors drive the satisfaction of citizens with governments' responses to COVID-19? *International Journal of Infectious Diseases 102*, 327–331.

Chen, C. W. and M. K. So (2006). On a threshold heteroscedastic model. *International Journal of Forecasting 22*(1), 73–89.

Chen, C. W. S. and S. Lee (2017). Bayesian causality test for integer-valued time series models with applications to climate and crime data. *Journal of the Royal Statistical Society, Series C 66*, 797–814.

Chen, Y., W. K. Härdle, and U. Pigorsch (2010). Localized realized volatility modeling. *Journal of the American Statistical Association 105*(492), 1376–1393.

Chernozhukov, V., H. Kasahara, and P. Schrimpf (2021). Causal impact of masks, policies, behavior on early COVID-19 pandemic in the US. *Journal of Econometrics 220*(1), 23–62.

Conrad, C. and B. R. Haag (2006). Inequality constraints in the fractionally integrated GARCH model. *Journal of Financial Econometrics 4*(3), 413–449.

Cui, Y., Q. Li, and F. Zhu (2020). Flexible bivariate Poisson integer-valued GARCH model. *Annals of the Institute of Statistical Mathematics 72*(6), 1449–1477.

Dandekar, R. and G. Barbastathis (2020). Quantifying the effect of quarantine control in Covid-19 infectious spread using machine learning. *medRxiv*.

Darolles, S., G. Le Fol, Y. Lu, and R. Sun (2019). Bivariate integer-autoregressive process with an application to mutual fund flows. *Journal of Multivariate Analysis 173*, 181–203.

Davis, R. A. and W. T. Dunsmuir (2016). State space models for count time series. *Handbook of Discrete-Valued Time Series. Chapman and Hall/CRC 1*, 121–144.

Davis, R. A., K. Fokianos, S. H. Holan, H. Joe, J. Livsey, R. Lund, V. Pipiras, and N. Ravishanker (2021). Count time series: A methodological review. *Journal of the American Statistical Association 116*, 1–15.

Diebold, F. X. (1986). Comment on modelling the persistence of conditional variance. *Econometric Reviews 5*(1), 51–56.

Engle, R. F. and T. Bollerslev (1986). Modelling the persistence of conditional variances. *Econometric reviews 5*(1), 1–50.

Famoye, F. and K. P. Singh (2006). Zero-inflated generalized Poisson regression model with an application to domestic violence data. *Journal of Data Science 4*, 117–130.

Faria, N. R., T. A. Mellan, C. Whittaker, I. M. Claro, D. d. S. Candido, S. Mishra, M. A. Crispim, F. C. Sales, I. Hawryluk, J. T. McCrone, et al. (2021). Genomics and epidemiology of the P. 1 SARS-CoV-2 lineage in Manaus, Brazil. *Science 372*(6544), 815–821.

Ferland, R., A. Latour, and D. Oraichi (2006). Integer-valued GARCH process. *Journal of Time Series Analysis 27*, 923–942.

Fokianos, K., B. Støve, D. Tjøstheim, and P. Doukhan (2020). Multivariate count autoregression. *Bernoulli 26*, 471–499.

Fokianos, K. and D. Tjøstheim (2011). Log-linear Poisson autoregression. *Journal of Multivariate Analysis 102*, 563–578.

Fokianos, K. and D. Tjøstheim (2012). Nonlinear Poisson autoregression. *Annals of the Institute of Statistical*

Mathematics (AISM) 64, 1205–1225.

Gelman, A., G. O. Roberts, and W. R. Gilks (1996). Efficient Metropolis jumping rules. In J. M. Bernardo, J. O. Berger, A. P. Dawid, and A. F. M. Smith (Eds.), *Bayesian Statistics*, pp. 599–608. Oxford University Press, Oxford.

Granger, C. W. (1980). Long memory relationships and the aggregation of dynamic models. *Journal of Econometrics 14*(2), 227–238.

Granger, C. W. and R. Joyeux (1980). An introduction to long-memory time series models and fractional differencing. *Journal of Time Series Analysis 1*(1), 15–29.

Gupta, P. L., R. C. Gupta, and R. C. Tripathi (1996). Analysis of zero-adjusted count data. *Computational Statistics & Data Analysis 23*(2), 207–218.

Han, X., Y. Zhu, Y. Zhang, and Y. Chen (2022). Policy effectiveness on the global COVID-19 pandemic and unemployment outcomes: A large mixed frequency spatial approach. *Available at SSRN 4049509*.

Hsiang, S., D. Allen, S. Annan-Phan, K. Bell, I. Bolliger, T. Chong, H. Druckenmiller, L. Y. Huang, A. Hultgren, E. Krasovich, et al. (2020). The effect of large-scale anti-contagion policies on the COVID-19 pandemic. *Nature 584*(7820), 262–267.

Hurst, H. E. (1951). Long-term storage capacity of reservoirs. *Transactions of the American Society of Cvil Engineers 116*(1), 770–799.

Jiang, F., Z. Zhao, and X. Shao (2020). Time series analysis of COVID-19 infection curve: A change-point perspective. *Journal of Econometrics*.

Kılıç, R. (2011). Long memory and nonlinearity in conditional variances: A smooth transition FIGARCH model. *Journal of Empirical Finance 18*(2), 368–378.

Lamoureux, C. G. and W. D. Lastrapes (1990). Persistence in variance, structural change, and the GARCH model.

Journal of Business & Economic Statistics 8, 225–234.

Lee, S., Y. Lee, and C. W. S. Chen (2016). Parameter change test for zero-inflated generalized Poisson autoregressive models. *Statistics 50*, 540–557.

Li, S. and O. Linton (2021). When will the Covid-19 pandemic peak? *Journal of Econometrics 220*(1), 130–157.

Lin, Q.-S., T.-J. Hu, and X.-H. Zhou (2020). Estimating the daily trend in the size of the COVID-19 infected population in wuhan. *Infectious Diseases of Poverty 9*(1), 1–8.

Liu, J. S. (2001). *Monte Carlo strategies in scientific computing*, Volume 10. Springer: New York.

Livsey, J., R. Lund, S. Kechagias, and V. Pipiras (2018). Multivariate integer-valued time series with flexible autocovariances and their application to major hurricane counts. *The Annals of Applied Statistics 12*(1), 408–431.

Ludvigson, S. C., S. Ma, and S. Ng (2020). COVID-19 and the macroeconomic effects of costly disasters. Technical report, National Bureau of Economic Research.

Marcellino, M., J. H. Stock, and M. W. Watson (2006). A comparison of direct and iterated multistep AR methods for forecasting macroeconomic time series. *Journal of Econometrics 135*(1-2), 499–526.

Mecenas, P., R. T. d. R. M. Bastos, A. C. R. Vallinoto, and D. Normando (2020). Effects of temperature and humidity on the spread of COVID-19: A systematic review. *PLoS one 15*(9), e0238339.

Mikosch, T. and C. Stărică (2004). Nonstationarities in financial time series, the long-range dependence, and the IGARCH effects. *Review of Economics and Statistics 86*(1), 378–390.

Qiu, Y., X. Chen, and W. Shi (2020). Impacts of social and economic factors on the transmission of coronavirus disease 2019 (COVID-19) in China. *Journal of Population Economics 33*(4), 1127–1172.

Quoreshi, A. S. (2014). A long-memory integer-valued time series model, INARFIMA, for financial application.

Quantitative Finance 14(12), 2225–2235.

Quoreshi, A. S. (2017). A bivariate integer-valued long-memory model for high-frequency financial count data. *Communications in Statistics-Theory and Methods 46*(3), 1080–1089.

Roy, A. and S. Karmakar (2021). Time-varying auto-regressive models for count time-series. *Electronic Journal of Statistics 15*(1), 2905–2938.

Segnon, M. and M. Stapper (2019). Long memory conditional heteroscedasticity in count data. Technical report, Center for Quantitative Economics (CQE), University of Muenster.

Shi, P., Y. Dong, H. Yan, C. Zhao, X. Li, W. Liu, M. He, S. Tang, and S. Xi (2020). Impact of temperature on the dynamics of the COVID-19 outbreak in china. *Science of the Total Environment 728*, 138890.

Taniguchi, M. and Y. Kakizawa (2000). *Asymptotic theory of statistical inference for time series*. Springer Science & Business Media.

Vaidyanathan, G. (2021). Coronavirus variants are spreading in India—what scientists know so far. *Nature 593*(7859), 321–322.

Volz, E., S. Mishra, M. Chand, J. C. Barrett, R. Johnson, L. Geidelberg, W. R. Hinsley, D. J. Laydon, G. Dabrera, Á. O'Toole, et al. (2021). Assessing transmissibility of SARS-CoV-2 lineage b. 1.1. 7 in England. *Nature 593*(7858), 266–269.

Xu, X., Y. Chen, C. W. Chen, and X. Lin (2020). Adaptive log-linear zero-inflated generalized Poisson autoregressive model with applications to crime counts. *The Annals of Applied Statistics 14*(3), 1493–1515.

Zhu, F. (2011). A negative binomial integer-valued GARCH model. *Journal of Time Series Analysis 32*, 54–67.

Xiaofei Xu

School of Mathematics and Statistics, Wuhan University, Wuhan, 430072, Hubei, People's Republic of China

REFERENCES

E-mail: xiaofeix@whu.edu.cn

Yijiong Zhang

Department of Mathematics, National University of Singapore, 21 Lower Kent Ridge Road, Singapore

E-mail: zhang.yijiong@u.nus.edu

Yan Liu

Institute for Mathematical Science, and Faculty of Science and Engineering, Waseda University, 3-4-1 Okubo,

Shinjuku-ku, Japan

E-mail: liu@waseda.jp

Yuichi Goto

Faculty of Mathematics, Kyushu University, 744 Motooka Nishi-ku Fukuoka, Japan

E-mail: goto.yuichi.436@m.kyushu-u.ac.jp

Masanobu Taniguchi

Research Institute for Science and Engineering, Waseda University, 3-4-1 Okubo, Shinjuku-ku, Japan

E-mail: taniguchi@waseda.jp

Ying Chen

Department of Mathematics, National University of Singapore, 21 Lower Kent Ridge Road, Singapore

E-mail: matcheny@nus.edu.sg